

A mechanical analogue of Faraday’s law for waves in chiral elastic media

Finn J.P. Allison*, Özgür Selsil, Stewart G. Haslinger & Alexander B. Movchan

Department of Mathematical Sciences, University of Liverpool

February 21, 2024

Abstract

Faraday’s law on electromagnetic induction, one of the most fundamental laws of nature, indicates that a change of magnetic field through a coil wire induces a current in the wire. Electromagnetic induction has many paramount technological applications today, and provides the link between electric and magnetic fields, which is crucial to explain the existence of electromagnetic waves. In our quest to replicate Faraday’s law for mechanical systems, we design an infinite mass-spring “helix-like structure”, which consists of a helix and a central line, and implement Bloch-Floquet conditions to obtain travelling wave solutions to the proposed problem. The structure’s geometrical chirality is considered in conjunction with a dynamic chirality, introduced by placing gyroscopes along its central line. It is shown that the interplay between these two chiralities acts as a mechanical analogue of Faraday’s law, breaking the symmetry of the associated dispersion diagram.

1 Introduction

As is well known, the Floquet theory is concerned with the study of elliptic differential equations with periodic coefficients [1]. The mathematical background established by Floquet was translated to physics by Bloch’s seminal study on electron motion in crystals [2]. Nowadays, this theory plays a crucial role in the understanding of wave propagation in periodic structures (dielectric gratings [3], chiral media [4], thermoelastic structures [5] and platonic crystals [6] to count a few).

Mass-spring systems with massless springs that obey Hooke’s law [7] have been a modelling tool for countless applications in physics and engineering, originating back to Newton’s Principia in 1686 [8]. Newton’s model consisted of a one-dimensional system of identical masses equidistantly distributed along the direction of propagation. In fact, until the middle of the 18th century and the emergence of Euler’s work on the continuous string using partial differential equations, mass-spring systems were the singular tool used to understand the propagation of sound. It was only in the 19th century when a more sophisticated two-dimensional model by Vincent [9] was introduced to replicate Lord Kelvin’s lattice model that shed light on the propagation of electromagnetic waves.


To the best of our knowledge, three-dimensional modelling of a helix with a central line, what we call a “helix-like structure”, has not been studied in the literature. It may appear surprising that there are not many studies that employ linear mass-spring systems for the investigation of vibrations of three-dimensional structures. Though, it is important to remember that “lattice structures” possibly include these systems as atoms in a solid may be modelled as masses and their closest neighbour interactions by springs. Starting from the early 20th century, lattice vibrations have been excessively studied, predominantly, to understand them in chemical compounds, such as sodium chloride by Kellermann [10], and the interactions between electrons and lattice vibrations in metals by Migdal [11] and

*Corresponding author: F.Allison2@liverpool.ac.uk

superconductors by Eliashberg [12] in the mid-1900s. Simultaneously, the effect of defects in lattice vibrations, Montroll [13], Eshelby [14], attracted much attention, and created a new research direction. More recently, elastic waves, focusing on propagating modes, in lattice structures, as well as their filtering properties were examined by Martinsson & Movchan [15] and visualised by so-called “phononic bandgaps”. Jensen [16] investigated the vibrational response of finite periodic lattices that were subjected to periodic loading, devoting special attention to the response in frequency ranges with gaps in the band structure for the corresponding infinite periodic lattice.

Remarkably, a “helix-like structure” serves as a link between the celebrated law of electromagnetic induction of Faraday and its mechanical equivalent in elastic media. This structure is intrinsically chiral, and elastic waves in chiral media are characterized by their sensitivity to the handedness of the medium, which arises from the presence of asymmetric structural features. Within the last decade, a significant amount of work has been carried out on the analysis of geometrically chiral elastic solids and lattices [17–19], to create effective auxetic media (with negative Poisson’s ratio ν) [20–23], and generate negative diffraction [24, 25]. The vibrational behaviour of helical springs is well documented [26–29]. The propagation of both elastic and electromagnetic waves in helical waveguides has been widely investigated in the context of non-destructive evaluation [30–33], as hollow helical waveguides for medical and industrial regimes [34, 35], and even a helically corrugated waveguide, implemented for gyrotron travelling wave tubes, was shown to significantly enhance its frequency bandwidth [36, 37].

Our investigation on the discrete “helix-like structure” with dynamic chirality (also known as active chirality) is induced by a series of gyroscopic spinners. It is important to distinguish between dynamically chiral systems, associated with the gyroscopic action, and geometrically chiral static structures. A circular helix is an example of a geometrically chiral structure with constant band curvature and constant torsion. Dynamically chiral systems may be used in unidirectional wave steering, to create topological insulators [38–40]. The papers by Carta *et al.* [41, 42], include analysis of the dispersion properties of chiral periodic gyroscopic elastic systems, where the gyroscopic action is analogous to the action of a unidirectional magnetic field in photonic crystal structures. Indeed, we are able to demonstrate that the preferential direction of propagation can be inverted by reversing the vorticity of the spinners in relation to the handedness of the helix.

When writing this article, we felt that the typical methods of presenting eigenmodes, using either a series of still frames or referring to a video in the supplementary material, were insufficient in portraying the vibrational behaviour of the “helix-like structure”. Thus, we came up with a novel idea: to design a tool, an app, which would not only provide important context and exposition to the analysis, but enhance the reading experience. For this reason, we highly encourage the reader to download the Eigenglass application, available on App store and Google Play, and take time to explore the animations and three-dimensional representations hidden behind each figure with .

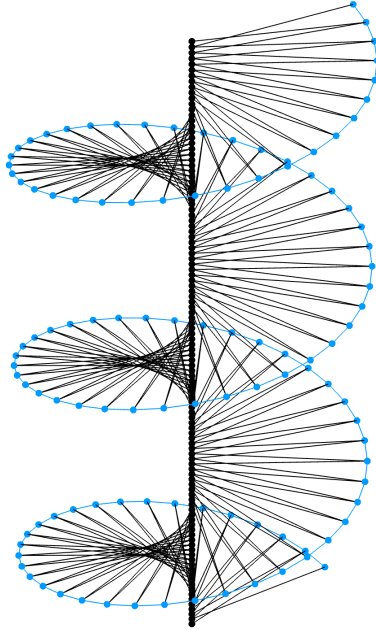



Figure 1: A portion of the infinite “helix-like structure”, with the helix itself depicted in blue. 

2 Problem formulation

We now formulate the problem in a discrete, infinite “helix-like structure”. We use this terminology not only because the structure is discrete but also because it consists of a helical rim as well as a central line, the latter having been introduced to add structural integrity.

In the generating unit cell $\Omega^{(0)}$, the building block of the construction, both the helix and central line have M masses attached to each other via massless springs, denoted by $m_{h,k}^{(0)}$ and $m_{c,k}^{(0)}$, $k = 1, \dots, M$, where subscripts h and c stand for helix and central, respectively. In addition, each mass on the helix is attached to two masses on the central line, more precisely $m_{h,k}^{(0)}$ is connected to both $m_{c,k\pm 1}^{(0)}$. An infinite three-dimensional “helix-like structure” is thus constructed by stacking $\Omega^{(0)}$ vertically along the positive and negative z -axis; we enumerate the masses in the proceeding/preceding unit cells as $m^{(j)} \in \Omega^{(j)}$, $j \in \mathbb{Z}_{+/-}$, respectively. We present a sample configuration in Figure 1, with springs depicted as straight lines for visual simplicity.

Representing the displacements of masses $m_{n,k}^{(j)}$ by $\mathbf{u}_{n,k}^{(j)}$, $j \in \mathbb{Z}, k = 1, \dots, M, n = h, c$, we set the Bloch-Floquet condition as

$$\mathbf{u}_{n,k}^{(j)} = e^{iKjd} \mathbf{u}_{n,k}^{(0)}, \quad j \in \mathbb{Z},$$

where d is the height of the unit cell, that is the pitch of the helix, and K is the wavenumber acting solely in the z -direction. Thus, referring to Figure 2, we have

$$\mathbf{u}_{h,1}^{(1)} = e^{iKd} \mathbf{u}_{h,1}^{(0)}, \quad \mathbf{u}_{h,M}^{(-1)} = e^{-iKd} \mathbf{u}_{h,M}^{(0)}, \quad \mathbf{u}_{c,1}^{(1)} = e^{iKd} \mathbf{u}_{c,1}^{(0)}, \quad \mathbf{u}_{c,M}^{(-1)} = e^{-iKd} \mathbf{u}_{c,M}^{(0)}.$$

To establish the governing equations, we begin with considering the masses on the helix that are connected only to other masses within $\Omega^{(0)}$. In general, the linearised force $\mathbf{F}_{i,j}$ between the i^{th} and j^{th} masses is given by the (responding force version of) Hooke’s law

$$\mathbf{F}_{i,j} = -\kappa_{i,j} [\mathbf{e}_{i,j}^{(0)} \cdot (\mathbf{u}_i - \mathbf{u}_j)] \mathbf{e}_{i,j}^{(0)},$$

where $\kappa_{i,j}$ is the stiffness of the spring between the two masses, $\mathbf{e}_{i,j}^{(0)}$ is the unit vector in the direction from mass i to j at equilibrium, and \mathbf{u}_i and \mathbf{u}_j are small displacements of the respective masses. Therefore,

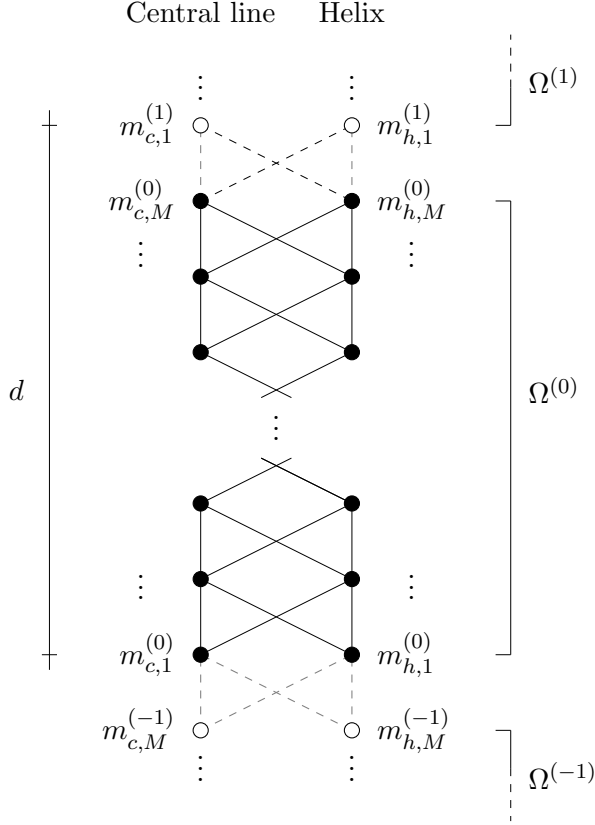



Figure 2: An unwound two-dimensional representation of the infinite (three-dimensional) helix-like structure. The dashed lines indicate the connections between the generating unit cell $\Omega^{(0)}$ and its repeated copies below and above, namely the neighbouring unit cells $\Omega^{(-1)}$ and $\Omega^{(1)}$. 

the forces exerted on masses $m_{h,k}^{(0)}$ by $m_{h,k\pm 1}^{(0)}$ on the helix and on masses $m_{c,k}^{(0)}$ by $m_{c,k\pm 1}^{(0)}$ on the central line are given by

$$\mathbf{F}_{(n,k),l} = -\kappa_{(n,k),l} \left[\frac{\mathbf{p}_{n,l} - \mathbf{p}_{n,k}}{|\mathbf{p}_{n,l} - \mathbf{p}_{n,k}|} \cdot (\mathbf{u}_{n,k} - \mathbf{u}_{n,l}) \right] \frac{\mathbf{p}_{n,l} - \mathbf{p}_{n,k}}{|\mathbf{p}_{n,l} - \mathbf{p}_{n,k}|}, \quad k = 2, \dots, M-1, l = k \pm 1, \quad (2.1)$$

for $n = h, c$. For the cross interactions between the masses on the helix and the central line, still within the generating unit cell, we take into account both forces exerted on the mass $m_{h,k}$ by the masses $m_{c,k\pm 1}$:

$$\mathbf{F}_{(h,k),(c,l)} = -\kappa_{(h,k),(c,l)} \left[\frac{\mathbf{p}_{c,l} - \mathbf{p}_{h,k}}{|\mathbf{p}_{c,l} - \mathbf{p}_{h,k}|} \cdot (\mathbf{u}_{h,k} - \mathbf{u}_{c,l}) \right] \frac{\mathbf{p}_{c,l} - \mathbf{p}_{h,k}}{|\mathbf{p}_{c,l} - \mathbf{p}_{h,k}|}, \quad k = 2, \dots, M-1, l = k \pm 1. \quad (2.2)$$

Needless to say, the force exerted on the mass $m_{c,k}$ by $m_{h,k\pm 1}$ is $\mathbf{F}_{(c,k),(h,l)} = -\mathbf{F}_{(h,k),(c,l)}$. In (2.1), (2.2), the position vectors for each mass on the helical rim are given by

$$\mathbf{p}_{h,k} = \left(\alpha \cos \frac{2\pi(k-1)}{M}, \alpha \sin \frac{2\pi(k-1)}{M}, \frac{d(k-1)}{M} \right), \quad k = 1, \dots, M,$$

where α is the radius of the helix, and, clearly, $\mathbf{p}_{c,k} = (0, 0, d(k-1)/M)$, $k = 1, \dots, M$.

The equations of motion for the $2(M-2)$ masses, which have no connections outside $\Omega^{(0)}$, may thus be written as follows

$$\ddot{\mathbf{u}}_{h,k} - \mathcal{F}_{(h,k),k+1} - \mathcal{F}_{(h,k),k-1} - \mathcal{F}_{(h,k),(c,k+1)} - \mathcal{F}_{(h,k),(c,k-1)} = \mathbf{0}, \quad (2.3)$$

$$\ddot{\mathbf{u}}_{c,k} - \mathcal{F}_{(c,k),k+1} - \mathcal{F}_{(c,k),k-1} - \mathcal{F}_{(c,k),(h,k+1)} - \mathcal{F}_{(c,k),(h,k-1)} - \mathcal{G}\omega \mathbf{R} \dot{\mathbf{u}}_{c,k} = \mathbf{0}, \quad (2.4)$$

for $k = 2, \dots, M - 1$, where $\mathcal{F}_{(n,k),\cdot} = \mathbf{F}_{(n,k),\cdot}/m_{n,k}$, and here and hereafter, dot on top of the variable denotes the time derivative. We give the forces exerted on the remaining four masses $m_{c,M}^{(0)}$, $m_{h,M}^{(0)}$, $m_{c,1}^{(0)}$ and $m_{h,1}^{(0)}$ inside the generating unit cell by masses that lie outside $\Omega^{(0)}$, explicitly in the Supplementary Material, and thus we may write the remaining governing equations as

$$\begin{aligned}
\ddot{\mathbf{u}}_{c,1} - \mathcal{F}_{(c,1),2} - \mathcal{F}_{(c,1),(h,2)} - \mathcal{F}_{(c,1),M}^{(0,-1)} - \mathcal{F}_{(c,1),(h,M)}^{(0,-1)} - \mathcal{G}\omega\mathbf{R}\dot{\mathbf{u}}_{c,1} &= \mathbf{0}, \\
\ddot{\mathbf{u}}_{c,M} - \mathcal{F}_{(c,M),M-1} - \mathcal{F}_{(c,M),(h,M-1)} - \mathcal{F}_{(c,M),1}^{(0,1)} - \mathcal{F}_{(c,M),(h,1)}^{(0,1)} - \mathcal{G}\omega\mathbf{R}\dot{\mathbf{u}}_{c,M} &= \mathbf{0}, \\
\ddot{\mathbf{u}}_{h,1} - \mathcal{F}_{(h,1),2} - \mathcal{F}_{(h,1),(c,2)} - \mathcal{F}_{(h,1),M}^{(0,-1)} - \mathcal{F}_{(h,1),(c,M)}^{(0,-1)} &= \mathbf{0}, \\
\ddot{\mathbf{u}}_{h,M} - \mathcal{F}_{(h,M),M-1} - \mathcal{F}_{(h,M),(c,M-1)} - \mathcal{F}_{(h,M),1}^{(0,1)} - \mathcal{F}_{(h,M),(c,1)}^{(0,1)} &= \mathbf{0},
\end{aligned} \tag{2.5}$$

where, once again, \mathcal{F} denotes relevant forces normalised by the associated masses. In equations (2.4) and (2.5)_{1,2}, $\mathcal{G} = \gamma/m_c$ with $\gamma > 0$ being the so-called spinner constant, and \mathbf{R} is the rotation matrix describing the in-plane vorticity effect induced by the gyroscope

$$\mathbf{R} = \begin{pmatrix} 0 & \pm 1 & 0 \\ \mp 1 & 0 & 0 \\ 0 & 0 & 1 \end{pmatrix}. \tag{2.6}$$

The presence of the terms with the rotation matrix \mathbf{R} in equations (2.4) and (2.5)_{1,2} are the mathematical equivalent of attaching a series of gyroscopic spinners to the central line masses and thus injecting dynamic chirality into the geometrically chiral “helix-like structure”. As the helix presented here has a right-handedness, the attached gyroscopes may either spin in the same direction (counterclockwise) or opposite (clockwise); the first choice of signs in the matrix \mathbf{R} would describe a vorticity effect in agreement with the chirality of the helix. We also inform the reader that the superscript now denotes the interaction between the generating unit cell $\Omega^{(0)}$ and the proceeding/preceding unit cells $\Omega^{(1)}/\Omega^{(-1)}$.

Assuming time-harmonic solutions with angular frequency ω , we use governing equations (2.3) - (2.5) to construct a stiffness matrix of size $6M = 3 \times 2M$ (number of dimensions \times number of masses, remembering that there are M masses on both the helix and central line), and determine the eigenfrequencies and eigenmodes for a given wavenumber K . Through the numerical assembly of dispersion diagrams, the relationship between eigenfrequency and wavenumber may be illustrated and analysed. Although the appearance of the dispersion diagram will change significantly depending on the tuning imposed, there are always four sets of branches present, whose associated eigenmodes correspond to radial or longitudinal vibrations, either on the helix or central line.

3 Mechanical analogue of Faraday’s law

As an illustration, we locate $M = 12$ masses on both the helix and central line, and impose a small pitch height of $d = 0.5$. We may tune the structure to elicit specific vibrational behaviour by stiffening the radial and central springs, and making the central line of masses significantly heavier than the ones on the helix. Under this tuning, we demonstrate that injecting dynamic chirality along the central line of the “helix-like structure” (with spinner constant $\gamma = 10$) breaks the symmetry of the associated dispersion diagram. Using the Eigenglass app, it is apparent that the addition of clockwise-spinning gyroscopes produces a shift of the dispersion curves to the right, specifically the ones describing radial shearing modes on the central line; to emphasise this shift, dispersion curves obtained from a “helix-like structure” with no gyroscopes is superimposed in red (see Figure 3(a)). Also referring to the same figure, we note that the branches associated with longitudinal modes on the helix and central line are unaffected by the addition of the gyroscopes. A shifting, in addition to a degree of skewing, also occurs for the higher frequency branches associated with radial modes on the helix, depicted in Figure 3(b). In fact, the amount of shift we observe is proportional to the number of gyroscopes, depicted in blue in Figure 3(c),

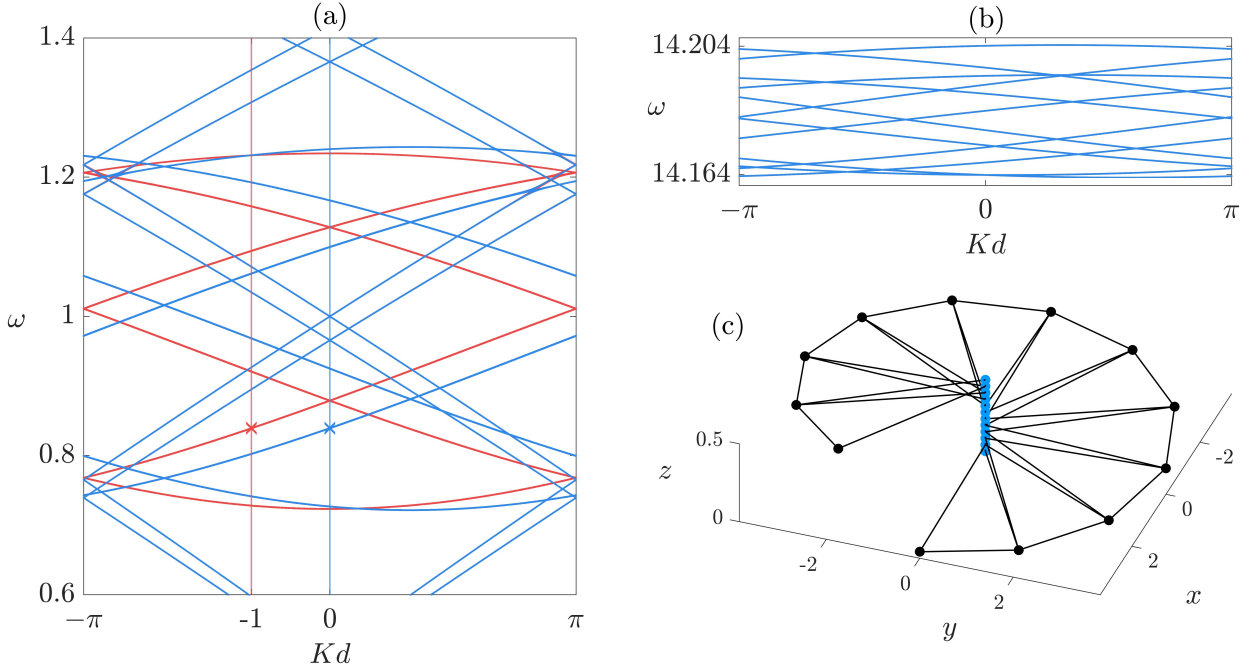



Figure 3: (a) A focused section of the dispersion diagram for the “helix-like structure” with gyroscopes attached to the masses on the central line for $\gamma = 10$. Red dispersion branches have been superimposed to indicate the position of the dispersion curves before the introduction of the gyroscopes. (b) Part of the same dispersion diagram given in (a), focusing on the higher-frequency branches associated with radial modes on the helix. (c) The generating unit cell of the infinite “gyrocore helix”. Using the Eigenglass app, one can see how the dispersion curves translate across the diagram as more gyroscopes are attached to the central line. 

we attach to the central line. We remark that only the generating unit cell is presented in Figure 3(c), therefore, with each gyroscope introduced in the animation, there are in fact infinitely many spinners being attached to the central line of the “gyrocore helix”.

Interestingly, a leftward shift of the dispersion curves may be visible if the gyroscopes spin in agreement with the chirality of the helix, or, in this case, counterclockwise. Indeed, the vorticity of the gyroscopic spinner, in relation to the handedness of the helix, affects the direction of propagation of the travelling wave. It is apparent that the interplay between these two chiralities acts as a mechanical analogue of Faraday’s law, whereby the direction of current may be determined by the polarisation of the magnetic field. Under the influence of a physically chiral object, the gyroscope, it is shown that the handedness of the helix breaks the symmetry of the associated dispersion diagram. The split eigenfrequencies along $Kd = 0$ may be determined from the eigenfrequency ω_0 , that was originally paired before the introduction of the gyroscopes, and the group velocity $V_g = d\omega/dK$ as

$$\omega - \omega_0 = \mp \tilde{\mathcal{G}} V_g. \quad (3.1)$$

Here, $\tilde{\mathcal{G}}(\mathcal{G}, M) \approx \gamma/10$, and the choice of sign on the right-hand side of equation (3.1) above determines the lower or higher split eigenfrequency, respectively.

Each split eigenfrequency indicates a separate eigenmode: a left- and a right-travelling wave, dependent on the respective branch they belong to. A natural curiosity is whether the shifting of the dispersion curves, and the subsequent splitting of paired eigenfrequencies along $Kd = 0$, emulates a change in dispersion for the associated eigenmodes. In essence, we would like to address the question: If the eigenfrequencies of a “gyrocore helix” at $Kd = 0$ coincide with the “helix-like structure” for, say, $Kd = -1$, would there also be correspondence between their eigenmodes? In Figure 4, we plot a bird’s

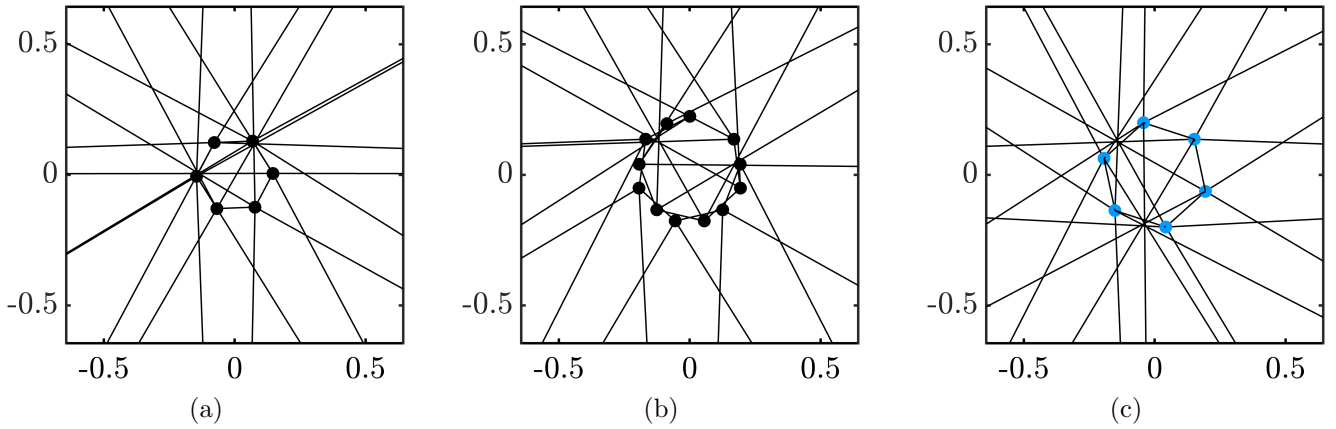



Figure 4: All three figures are in bird’s eye view. Due to the small pitch value, the z -axis scale for the three-dimensional visualisations is increased for easier viewing. All modes display shear radial vibrations on the central line. (a) $Kd = 0$ with no gyroscopes on the central line. (b) $Kd = -1$ with no gyroscopes on the central line. (c) $Kd = 0$ for a “gyrocore helix”. 

eye view for the following cases:

- (a) one of the paired eigenmodes at $Kd = 0$ for a “helix-like structure”,
- (b) the eigenmode corresponding to the lower-frequency branch at $Kd = -1$ for a “helix-like structure” (see the red marker in Figure 3(a)),
- (c) the eigenmode with an identical eigenfrequency as in (b) above, obtained at $Kd = 0$ for a “gyrocore helix” (see the blue marker in Figure 3(a)).

We choose $Kd = -1$ for the “helix-like structure” in order to target the identical eigenfrequencies which lie on the line $Kd = 0$ in Figure 3(a). The base case displayed in Figure 4(a) is clearly a standing mode, formed by the interference of a left- and a right-travelling wave. From above, the central line masses overlap to form a hexagon, which appears to oscillate in size as the shear displacements fluctuate. Introducing negative dispersion into the system creates latency between the central-line masses (from top to bottom), which induces a downward propagating wave. From above, this latency means the central masses no longer overlap and the central polygon appears to rotate in place, as evident in Figure 4(b). Finally, in Figure 4(c), we target the same eigenmode but for a gyroscopic central line of masses, with zero dispersion in the system. Indeed, the shear radial eigenmodes of a “gyrocore helix” closely resemble the dispersive eigenmodes of an identical structure that does not possess a dynamic chirality. Despite a difference in wavenumber, a downward travelling wave is visible in both (b) and (c), and the resemblance between the two figures is distinct. The juxtaposition between a physical and geometric chirality generates dispersion within the system, as is now evident by the associated eigenmodes. For a “gyrocore helix” with vorticity in agreement with the geometric chirality, we observe a left-shifting of the dispersion curves and an upward propagation of the mass vibrations.

4 Acknowledgements

F. J. P. Allison gratefully acknowledges the Engineering and Physical Sciences Research Council [grant number EP/V52007X/1] for funding his studentship.

References

- [1] G. Floquet, “Sur les équations différentielles linéaires à coefficients périodiques,” in *Annales scientifiques de l’École normale supérieure*, vol. 12, pp. 47–88, 1883.

- [2] F. Bloch, “Über die quantenmechanik der elektronen in kristallgittern,” *Zeitschrift für physik*, vol. 52, no. 7-8, pp. 555–600, 1929.
- [3] P. S. J. Russell, “Optics of Floquet-Bloch waves in dielectric gratings,” *Applied Physics B*, vol. 39, pp. 231–246, 1986.
- [4] G. Y. Slepyan, A. Gurevich, and S. Maksimenko, “Floquet-Bloch waves in periodic chiral media,” *Physical Review E*, vol. 51, no. 3, p. 2543, 1995.
- [5] I. Jones and A. Movchan, “Bloch-Floquet waves and controlled stop bands in periodic thermo-elastic structures,” *Waves in Random and Complex Media*, vol. 17, no. 4, pp. 429–438, 2007.
- [6] R. McPhedran, A. Movchan, and N. Movchan, “Platonic crystals: Bloch bands, neutrality and defects,” *Mechanics of materials*, vol. 41, no. 4, pp. 356–363, 2009.
- [7] R. Hooke, “1678: De potentia restitutiva, or of spring explaining the power of springing bodies.”
- [8] I. Newton, “Philosophiae naturalis principia mathematica, Streater, London, 1686.”
- [9] J. Vincent, “LX. on the construction of a mechanical model to illustrate Helmholtz’s theory of dispersion,” *The London, Edinburgh, and Dublin Philosophical Magazine and Journal of Science*, vol. 46, no. 283, pp. 557–563, 1898.
- [10] E. Kellermann, “Theory of the vibrations of the sodium chloride lattice,” *Philosophical Transactions of the Royal Society of London. Series A, Mathematical and Physical Sciences*, vol. 238, no. 798, pp. 513–548, 1940.
- [11] A. Migdal, “Interaction between electrons and lattice vibrations in a normal metal,” *Sov. Phys. JETP*, vol. 7, no. 6, pp. 996–1001, 1958.
- [12] G. Eliashberg, “Interactions between electrons and lattice vibrations in a superconductor,” *Sov. Phys. JETP*, vol. 11, no. 3, pp. 696–702, 1960.
- [13] E. W. Montroll and R. B. Potts, “Effect of defects on lattice vibrations,” *Physical Review*, vol. 100, no. 2, p. 525, 1955.
- [14] J. Eshelby, “The continuum theory of lattice defects,” in *Solid state physics*, vol. 3, pp. 79–144, Elsevier, 1956.
- [15] P. Martinsson and A. Movchan, “Vibrations of lattice structures and phononic band gaps,” *Quarterly Journal of Mechanics and Applied Mathematics*, vol. 56, no. 1, pp. 45–64, 2003.
- [16] J. S. Jensen, “Phononic band gaps and vibrations in one- and two-dimensional mass-spring structures,” *Journal of sound and Vibration*, vol. 266, no. 5, pp. 1053–1078, 2003.
- [17] R. K. Pal and M. Ruzzene, “Edge waves in plates with resonators: an elastic analogue of the quantum valley hall effect,” *New Journal of Physics*, vol. 19, no. 2, p. 025001, 2017.
- [18] T. Frenzel, M. Kadic, and M. Wegener, “Three-dimensional mechanical metamaterials with a twist,” *Science*, vol. 358, no. 6366, pp. 1072–1074, 2017.
- [19] A. Bacigalupo and L. Gambarotta, “Simplified modelling of chiral lattice materials with local resonators,” *International Journal of Solids and Structures*, vol. 83, pp. 126–141, 2016.
- [20] C. S. Ha, M. E. Plesha, and R. S. Lakes, “Chiral three-dimensional lattices with tunable poisson’s ratio,” *Smart Materials and Structures*, vol. 25, no. 5, p. 054005, 2016.
- [21] A. Spadoni and M. Ruzzene, “Elasto-static micropolar behavior of a chiral auxetic lattice,” *Journal of the Mechanics and Physics of Solids*, vol. 60, no. 1, pp. 156–171, 2012.

- [22] D. Prall and R. Lakes, “Properties of a chiral honeycomb with a Poisson’s ratio of -1 ,” *International Journal of Mechanical Sciences*, vol. 39, no. 3, pp. 305–314, 1997.
- [23] J. N. Grima, R. Gatt, and P.-S. Farrugia, “On the properties of auxetic meta-tetrachiral structures,” *physica status solidi (b)*, vol. 245, no. 3, pp. 511–520, 2008.
- [24] R. Zhu, X. Liu, G. Hu, C. Sun, and G. Huang, “Negative refraction of elastic waves at the deep-subwavelength scale in a single-phase metamaterial,” *Nature communications*, vol. 5, no. 1, p. 5510, 2014.
- [25] D. Tallarico, N. V. Movchan, A. B. Movchan, and D. J. Colquitt, “Tilted resonators in a triangular elastic lattice: chirality, Bloch waves and negative refraction,” *Journal of the Mechanics and Physics of Solids*, vol. 103, pp. 236–256, 2017.
- [26] W. H. Wittrick, “On elastic wave propagation in helical springs,” *International Journal of Mechanical Sciences*, vol. 8, no. 1, pp. 25–47, 1966.
- [27] A. Hamza, S. Ayadi, and E. Hadj-Taïeb, “The natural frequencies of waves in helical springs,” *Comptes Rendus Mécanique*, vol. 341, no. 9-10, pp. 672–686, 2013.
- [28] A. Hamza, S. Ayadi, and E. Hadj-Taïeb, “Propagation of strain waves in cylindrical helical springs,” *Journal of Vibration and Control*, vol. 21, no. 10, pp. 1914–1929, 2015.
- [29] S. Sorokin, “Linear dynamics of elastic helical springs: asymptotic analysis of wave propagation,” *Proceedings of the Royal Society A: Mathematical, Physical and Engineering Sciences*, vol. 465, no. 2105, pp. 1513–1537, 2009.
- [30] F. Treyssède, “Numerical investigation of elastic modes of propagation in helical waveguides,” *The Journal of the Acoustical Society of America*, vol. 121, no. 6, pp. 3398–3408, 2007.
- [31] F. Treyssède, “Elastic waves in helical waveguides,” *Wave motion*, vol. 45, no. 4, pp. 457–470, 2008.
- [32] Y. Liu, Q. Han, C. Li, and H. Huang, “Numerical investigation of dispersion relations for helical waveguides using the scaled boundary finite element method,” *Journal of Sound and Vibration*, vol. 333, no. 7, pp. 1991–2002, 2014.
- [33] F. Treyssède and L. Laguerre, “Investigation of elastic modes propagating in multi-wire helical waveguides,” *Journal of sound and vibration*, vol. 329, no. 10, pp. 1702–1716, 2010.
- [34] Z. Menachem and M. Mond, “Infrared wave propagation in a helical waveguide with inhomogeneous cross section and applications,” *Progress In Electromagnetics Research*, vol. 61, pp. 159–192, 2006.
- [35] Z. Menachem and S. Tapuchi, “Helical waveguide with two bendings, and applications,” *Progress In Electromagnetics Research B*, vol. 26, pp. 115–147, 2010.
- [36] G. G. Denisov, V. L. Bratman, A. D. Phelps, and S. V. Samsonov, “Gyro-TWT with a helical operating waveguide: New possibilities to enhance efficiency and frequency bandwidth,” *IEEE transactions on plasma science*, vol. 26, no. 3, pp. 508–518, 1998.
- [37] W. He, K. Ronald, A. R. Young, A. W. Cross, A. D. Phelps, C. G. Whyte, E. G. Rafferty, J. Thomson, C. W. Robertson, D. C. Speirs, *et al.*, “Gyro-BWO experiments using a helical interaction waveguide,” *IEEE transactions on electron devices*, vol. 52, no. 5, pp. 839–844, 2005.
- [38] X. Ni, C. He, X.-C. Sun, X.-p. Liu, M.-H. Lu, L. Feng, and Y.-F. Chen, “Topologically protected one-way edge mode in networks of acoustic resonators with circulating air flow,” *New Journal of Physics*, vol. 17, no. 5, p. 053016, 2015.
- [39] R. Süsstrunk and S. D. Huber, “Observation of phononic helical edge states in a mechanical topological insulator,” *Science*, vol. 349, no. 6243, pp. 47–50, 2015.

- [40] M. Garau, G. Carta, M. Nieves, I. Jones, N. Movchan, and A. Movchan, “Interfacial waveforms in chiral lattices with gyroscopic spinners,” *Proceedings of the Royal Society A: Mathematical, Physical and Engineering Sciences*, vol. 474, no. 2215, p. 20180132, 2018.
- [41] G. Carta, D. Colquitt, A. Movchan, N. Movchan, and I. Jones, “One-way interfacial waves in a flexural plate with chiral double resonators,” *Philosophical Transactions of the Royal Society A*, vol. 378, no. 2162, p. 20190350, 2020.
- [42] G. Carta, D. Colquitt, A. Movchan, N. Movchan, and I. Jones, “Chiral flexural waves in structured plates: directional localisation and control,” *Journal of the Mechanics and Physics of Solids*, vol. 137, p. 103866, 2020.